On the Dynamics of a Vertically Driven Damped Planar Pendulum

M. V. Bartuccelli*, G. Gentile†, K. V. Georgiou*

* *Department of Mathematics and Statistics, University of Surrey, Guildford, GU2 7XH*
† *Dipartimento di Mathematica, Università di Roma Tre, Roma, I–00146, Italy*

August 29, 2000

Abstract

The dynamics of the planar pendulum with parametric vertical time-periodic forcing is considered. Analytical and numerical methods are employed to study the various dynamical features of the system. A rigorous analysis is presented in order to show that, in presence of friction, the upward equilibrium position becomes asymptotically stable when the period of the forcing is below an appropriate threshold; this is illustrated by performing numerical computations and advanced visualization techniques. Also the dynamics of the system far from its equilibrium points is systematically investigated by using Poincaré sections and phase portraits. The attractors and the associated basins of attraction are computed. Furthermore we calculate the Lyapunov exponents to show that for some parameter values the dynamics of the pendulum shows sensitivity to initial conditions.

1 Introduction

Over the last decades parametrically excited nonlinear oscillators have begun to be extensively studied, both theoretically and numerically. Their dynamics is generally very complicated even when only one and a half degrees of freedom are involved: this shows that the complex behaviour does not arise from a large number of variables, but from the nonlinearity of the equation of motion.

Below, a planar pendulum whose point of support (pivot) is subjected to vertical sinusoidal displacement is studied. This system has two equilibrium configurations: the downward position and the upward position. It is known that the upward equilibrium state can be made stable by subjecting the pivot to a harmonic vertical oscillation of appropriate frequency and amplitude: analytically this is obtained by the method of *averaging* (see Kapitsa [26], Landau and Lifshitz [29] or Percival and Richards [36]), which, however, is not completely satisfactory [8, 7].

Stephenson [41] in 1908 was the first who predicted theoretically this remarkable result, and the idea has reappeared in a number of subsequent studies (Ness [35]; Kalmus [25]; Pippard [37]; Leiber and Risken [30]; Koch *al.* [27, 32]; Michaelis [33]; Blackburn *et al.* [8]; Acheson [1, 2, 3]).

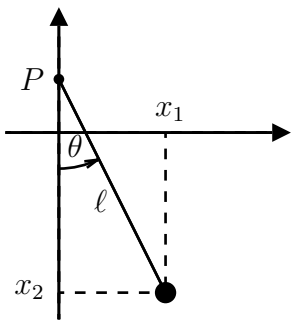

Figure 1: The pendulum with the point of support oscillating on a vertical line.

In this paper we employ analytical and numerical techniques to make detailed studies of such a system in presence of friction. We shall investigate the stability of both fixed points and study their basins of attraction when they are (asymptotically) stable.

We shall also investigate the existence of other attractors, and again determine the corresponding basins of attraction; analogous results for similar models can be found in literature [9, 11, 39, 40]. The results depend strongly upon the values of the parameters: both regular (smooth) and chaotic attractors can arise, but never simultaneously. A systematic study of all possible scenarios arising by varying the parameters values is certainly interesting, but we shall not perform it here, as we are interested rather in showing the complexity of features exhibited by the system. Furthermore we find also strong numerical evidence that in the cases we explicitly consider we find all attractors (by showing that the union of the basins of attraction fills all the phase space).

We compute the Lyapunov exponents to show sensitivity to initial conditions, thereby corroborating the fact that the system does possess the chaotic dynamics described above.

Numerical Poincaré sections [22, 38, 23] and phase portraits [12, 21, 6] have been employed to show that, according to appropriate parameters values, the motion of the pendulum can be either regular or chaotic. Some of the results we find are already been observed in literature (see below): in such cases there is complete agreement with our observations.

Visualization techniques [17] are used for further analysis of the dynamics of our system; generally computer animation techniques provide a great potential for illustrating properties of dynamical systems. We shall make use of MAPLE [20, 34] and other algebraic packages to show that, in the presence of damping, the upward fixed point becomes asymptotically stable.

A rigorous analysis proves that, in the presence of (even small) friction, the upward equilibrium position of the driven pendulum does indeed become stable if the period of the forcing is small enough, in excellent agreement with both numerical computations and graphic visualization.

2 A forced planar pendulum

A schematic of the pendulum is shown in Figure 1. A simple pendulum consisting of a point mass m at a distance ℓ, constrained to move in a vertical plane under the influence of gravity, oscillates about the pivot which is vertically forced at a distance $y_0(t) = b\cos\omega t$, where b and ω are the amplitude and frequency of the pivot motion.

The governing equation is deduced by introducing coordinates relative to the plane of motion of the pendulum and using a Lagrangian formulation. The coordinates of mass m are denoted by (x_1, x_2) and given by

$$x_1(t) = \ell\sin\theta(t)\,, \quad x_2(t) = y_0(t) - \ell\cos\theta(t)\,, \tag{2.1}$$

where θ is the (clockwise counted) angle that the pendulum forms with the vertical (oriented downward), and $y_0(t)$ is the prescribed vertical forcing. The Lagrangian for the system is then

$$\begin{aligned} \mathcal{L} &= \frac{1}{2}m\left(\ell^2\dot\theta^2 + 2\ell\ddot y_0(t)\cos\theta\right) + mg\ell\cos\theta \\ &= \frac{1}{2}m\ell^2\dot\theta^2 + mg\ell\cos\theta - m\ell b\omega^2\cos\theta\cos\omega t, \end{aligned} \tag{2.2}$$

where g is the gravitational constant. The governing equation of the system is given by :

$$\ddot\theta + \left(\frac{g}{\ell} - \frac{b\omega^2}{\ell}\cos\omega t\right)\sin\theta = 0. \tag{2.3}$$

By letting $\tau = \omega t$ we have

$$\ddot\theta + (\alpha - \beta\cos\tau)\sin\theta = 0, \qquad \alpha = \frac{g}{\ell\omega^2}, \qquad \beta = \frac{b}{\ell}. \tag{2.4}$$

This equation is referred to as the *vertically driven pendulum* equation: it is structurally identical to (2.3), but it is written in a generalised dimensionless form. It has the advantages that

1. of the original four parameters (g, ℓ, b, ω) only two (α, β) are left;

2. due to the dimensionless character of all the terms, it can be used to compare directly the dynamics of nonlinear, driven oscillators in any field, for example in mechanics, electrodynamics or solid state physics.

Since the system is 2π periodic in θ, the fixed points are $(0,0)$ and $(\pi,0)$. The $(0,0)$ fixed point corresponds to the downward state of the pendulum, while the $(\pi,0)$ corresponds to the upward state. Equation (2.4) can not be solved anaytically, but if we assume that θ remains near the equilibrium point throughout the motion, it may be linearised: linearization around $(0,0)$, by Taylor expansion, leads $\sin\theta$ to be approximated by θ, so that the equation of motion becomes

$$\ddot{\theta} + (\alpha - \beta\cos\tau)\,\theta = 0, \tag{2.5}$$

while linearization around $(\pi,0)$ leads $\sin\theta$ to be approximated by $\pi+\theta$, so that, by letting $\xi = \pi+\theta$, (2.4) reads as

$$\ddot{\xi} + (-\alpha + \beta\cos\tau)\,\xi = 0. \tag{2.6}$$

Equations (2.5,2.6) are called Mathieu's equations; they are second order homogenous non-autonomous linear differential equations with real periodic coefficients. Figure 2 shows that the solutions of Mathieu's equations, depending on the values of the parameters α and β, are either stable or unstable (bounded or unbounded). In Figure 2 we observe that if β is small there is an

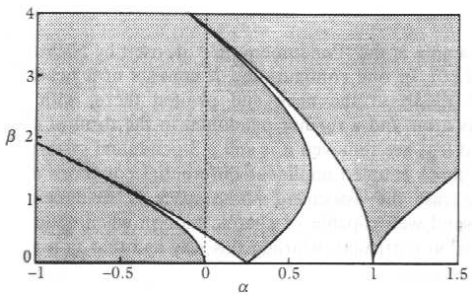

Figure 2: Stability diagram for Mathieu's equations (2.5,2.6). To the right of the dotted line ($\alpha = 0$), the $\theta = 0$ state is unstable in the shaded region, on the left the $\theta = \pi$ state is unstable in the shaded region. Only the region $\beta \geq 0$ is explicitly represented as the diagram is even in β.

instability region centered on $\alpha \approx 1/4$. If $\alpha = 0.5$ and $\beta = 0.1$ the downward state is stable, while if $\alpha = 0.25$ and $\beta = 0.1$ it is unstable; this carries over to the full system (2.4), as shown in Figure 3. Also if $\alpha = -0.1$ and $\beta = 0.545$ we are inside the stability region of the upward state of the

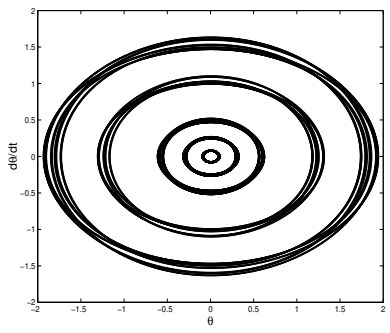

(a) Stable solutions of (2.4) using $\alpha = 0.5$ and $\beta = 0.1$.

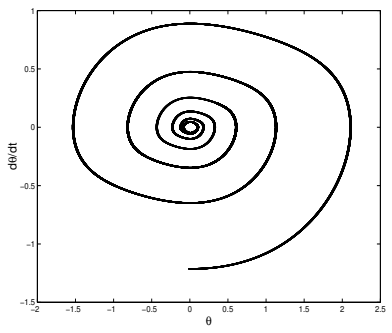

(b) An unstable solution of (2.4) using $\alpha = 0.25$ and $\beta = 0.1$.

Figure 3: Stabilility and instability of the the downward state of the pendulum described by (2.4).

pendulum, while if $\alpha = -0.2$ and $\beta = 0.1$ the upward state becomes unstable and the trajectories

move away from the fixed point; again this carries over to the full system, as illustrated in Figure 4.

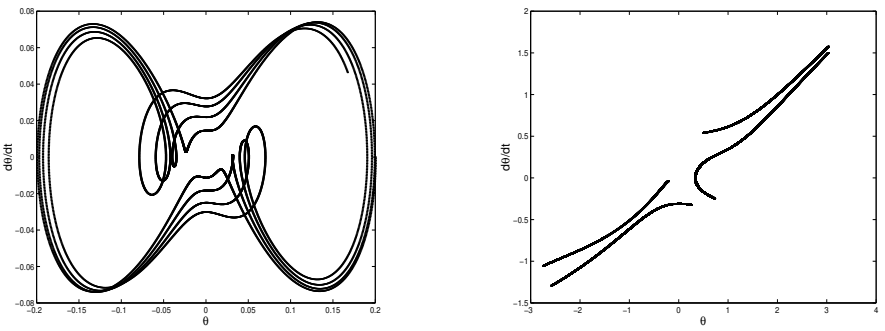

(a) Stable solution of (2.4) using $\alpha = -0.1$ and $\beta = 0.545$.

(b) Unstable solutions of (2.4) using $\alpha = -0.2$ and $\beta = 0.1$.

Figure 4: Stabilility and instability of the upward state of the pendulum described by (2.4).

The presence of friction, unavoidable in any physical context, leads to introduce a damping term into the equation of motion (2.4), which becomes

$$\ddot{\theta} + (\alpha - \beta \cos \tau) \sin \theta + \gamma \dot{\theta} = 0, \tag{2.7}$$

with $\gamma > 0$ denoting the *dissipation coefficient*.

The linearization of (2.7) around the two equilibrium points leads to the same equations (2.5) and (2.6) for the variables $\theta'(t) = e^{\gamma t/2}\theta(t)$ and $\xi'(t) = e^{\gamma t/2}\xi(t)$, respectively, provided that α is replaced with $\alpha' = \alpha - \gamma^2/4$ in both cases; see Jordan and Smith [24], Ch. 8. Therefore if γ is small enough (for practical purposes one can take γ as done below), for the values of α and β given above the behaviour of the linearized equations in presence of friction (for θ' and ξ') is the same of that of Mathieu's equations (for θ and ξ) obtained for $\gamma = 0$; it is important to note, however, that a stable equilibrium point for the linearized motion of θ' and ξ' becomes asymptotically stable for the linearized motion of the original variables θ and ξ. The stability chart of Mathieu's equation with damping was numerically determined by Leiber and Risken [30]; to compare (2.7) with equation (4) of [30] use that $\delta = 4\alpha$ and $\varepsilon = 2\beta$.

3 Trajectories in phase space and basins of attraction

Given an attractor, the most direct way of determining a basin of attraction is to numerically integrate the differential equation (2.7) for each possible initial point and record those initial conditions which eventually asymptote to the attractor (see also [8]). This approach has been used to generate high resolution basins containing as many as 1048576 (1024×1024 grid) initial conditions.

We have determined the basin of attraction for the upward and downward state for values of the parameters for which they are stable. A small target area of dimension 0.20×0.20 around the attractor was first specified. Points were then selected from the grid of initial conditions and for each one a fourth order Runge-Kutta integration routine was used to numerically integrate the system over an initial transient phase; the integration time step (time unit) was set at 0.1 (about one-sixthieth of the drive period). After this phase, which was typically 4000 time units, a further period of integration was specified and if at any time the solution entered the target area and remained there for several more time units it was assumed that that initial condition belonged to the basin of attraction for that attractor, since other attracting states were far away from the target area.

As an illustration of this method, consider the system (2.7) with $\alpha = -0.1$, $\beta = 0.545$ and $\gamma = 0.08$. For this case we have found that there are three coexisting attractors: the stationary state $(\theta, \dot{\theta}) = (\pi, 0)$, which corresponds to the upward position of the pendulum, and two other attractors

which correspond to rotating (running) solutions. We show in Figure 5a the basin of attraction for the stationary solution, and in Figure 5b the basin for the clockwise and anticlockwise running solutions. Any initially condition inside the black regions in Figure 5 will ultimately arrive at the corresponding attractor. Note that for each basin there are regions in which the structure seems to be factral [39]; for instance Fig. 5a reveals a dense core surrounded by fractal layers.

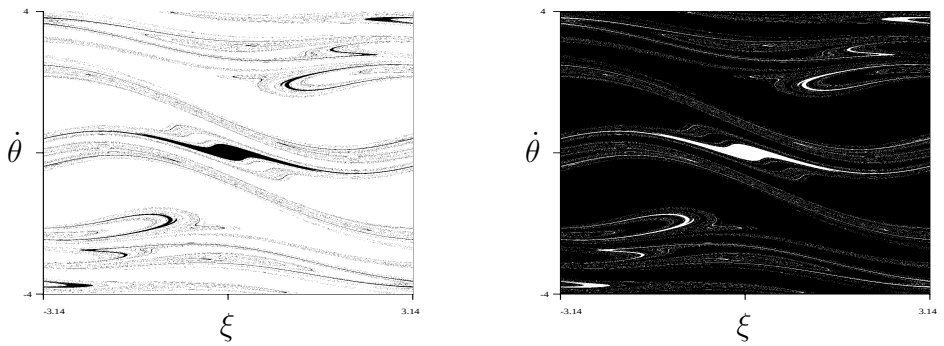

(a) Stationary solution.

(b) Rotating solutions.

Figure 5: Coexistence of three basins of attraction (in black) for the vertically driven pendulum with $\alpha = -0.1$, $\beta = 0.545$ and $\gamma = 0.08$; one has $\xi = \pi + \theta$.

We also investigated numerically the system (2.7) for the values of the parameters $\alpha = 0.5$, $\beta = 0.1$ and $\gamma = 0.03$. We have found that there are four coexisting attractors: the stationary state $(\theta, \dot{\theta}) = (0, 0)$, an oscillating solution, a clockwise running solution and a counterclockwise running solution. We show in Figure 6a the basin of attraction for the stationary solution, in Figure 6b the basin of attraction for the oscillating solution, finally in Figure 6c the basins of attraction for the clockwise and anticlockwise running solutions.

To characterise the attractors one can use a phase portrait in which the time variable is ignored, by projecting all trajectories on the 'phase space' $(\xi, \dot{\theta})$, with $\xi = \pi + \theta$, in the case of Figure 5, or $(\theta, \dot{\theta})$ in the case of Figure 6; practically this is accomplished by using DSTOOL.

For parameters values $\alpha = 0.5$, $\beta = 0.1$ and $\gamma = 0.03$ and for initial conditions inside the black region in Figure 6a, the trajectories converge to the fixed point $(\theta, \dot{\theta}) = (0, 0)$ as shown in Figure 7a. For the same parameters values and for initial conditions that are inside the black region in Figure 6b, an oscillatory behaviour can be observed after some transients: the trajectories converge to an oscillating orbit, which in this case is the attractor, as shown in Figure 7b. Finally for initial conditions that are inside the black region in Figure 6c, a clockwise running solution and a counterclockwise running solution can be observed; due to the symmetry of the phase space, each of these two attractors can be found by rotating the other by π.

Figures 7 show a phenomenon that is characteristic of nonlinear systems but cannot occur in linear systems. For the given system parameters $\alpha = 0.5$, $\beta = 0.1$ and $\gamma = 0.03$, there is a coexistence of four different attractors: depending on the initial conditions, trajectories converge towards one of these attractors (while for linear systems differences in initial conditions are damped out resulting in a single attractor).

We have also found that there is numerical evidence that these four coexisting attractors are the only attractors for the fixed parameters values. This was done by numerically integrating the system for each initial condition and recording (colored in black) those initial conditions which eventually asymptote to the attractors in Figures 7a,b. Any trajectory will ultimately end up to one of the attractors as shown numerically in Figure 6d, where the union of the four basins is represented.

Similarly for the system (2.7) with $\alpha = -0.1$, $\beta = 0.545$ and $\gamma = 0.08$, there is a coexistence of three different attractors: for initial conditions inside the black region in Figure 5a the trajectories converge to the fixed point attractor $(\theta, \dot{\theta}) = (\pi, 0)$, as shown in Figure 8a, while for initial conditions that are inside the black region in Figure 5b, a clockwise running solution and an anticlockwise running solution can be observed as shown in Figure 8b. Also in this case we found that these three attractors are the only attractors (the same picture as in Figure 6d is obtained by drawing simultaneously all the basins represented in Figure 5).

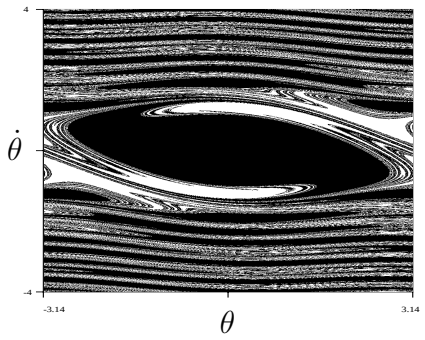

(a) Stationary solution.

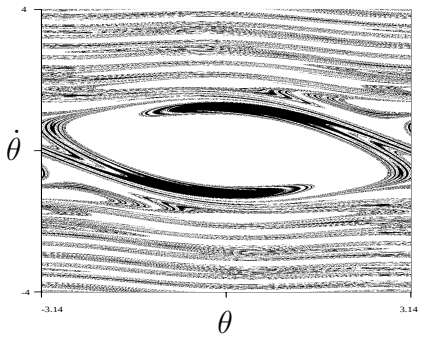

(b) Oscillating solution.

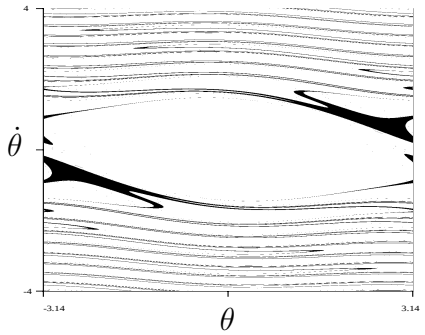

(c) Rotating solutions.

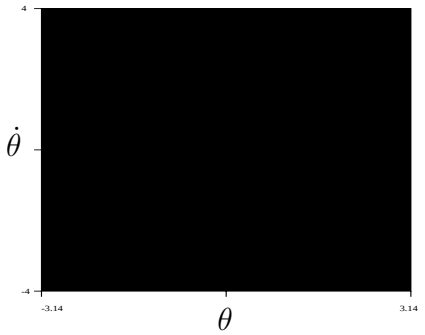

(d) Union of all basins.

Figure 6: Coexistence of four basins of attraction (in black) for the vertically driven pendulum with $\alpha = 0.5$, $\beta = 0.1$ and $\gamma = 0.03$.

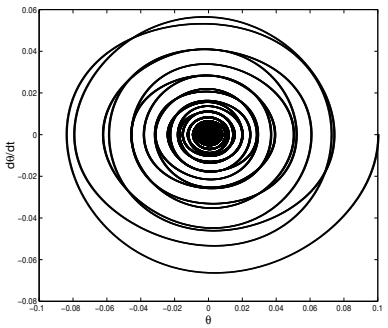

(a) A spiral orbit that goes toward the fixed point attractor.

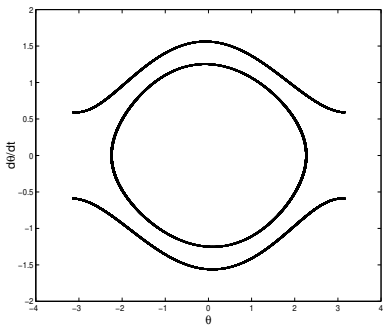

(b) Attractors for the oscillating and the two rotating solutions.

Figure 7: Attractors for the vertically driven pendulum with $\alpha = 0.5$, $\beta = 0.1$ and $\gamma = 0.03$.

For the parameters values $\alpha = 0.02$, $\beta = 0.35$ and $\gamma = 0.03$ the downward state and the upward state are both stables; in such a case we found that there are five coexistent attractors: the two stationary states $(0, 0)$ and $(\pi, 0)$ (if we use the coordinate θ), an oscillating solution, a clockwise running solution and a counterclockwise running solution; see Figure 9. The corresponding basins of attractions are given in Figure 10; again their union gives the entire phase space.

The parameters values considered so far are all inside the stability region in Figure 2. What happens, as a general rule, is that, if an equilibrium position is stable for Mathieu's equations

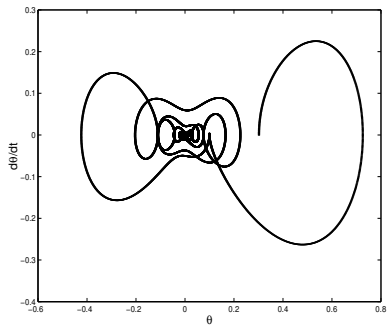

(a) A spiral orbit that goes toward the fixed point attractor.

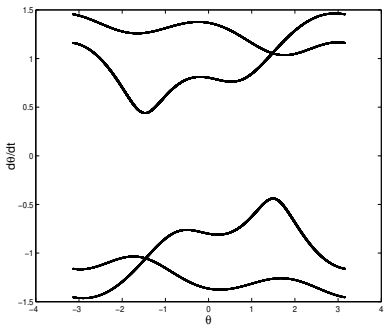

(b) Rotating clockwise and counterclockwise solutions.

Figure 8: Attractors for the vertically driven pendulum with $\alpha = -0.1$, $\beta = 0.545$ and $\gamma = 0.08$.

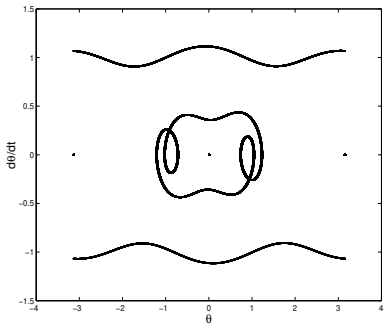

Figure 9: Attractors for the vertically driven pendulum with $\alpha = 0.02$, $\beta = 0.35$ and $\gamma = 0.03$.

(2.5) or (2.6), then it remains stable also for the nonlinear damped equation (2.7); this holds only approximately for negative values of α (see [30] for a detailed description of the stability diagram). In such cases one typically finds coexistence of several smooth attractors, like in the cases explicitly worked out above. The situation drastically changes when one takes values of the parameters for which the fixed points attractors are both unstable: in such cases new chaotic attractors appear, a phenomenon which is well known in literature [16, 8]; see Sect. 4.

4 Poincaré sections and strange attractors

It is well known that if a nonlinear dissipative system is driven by an external force, then depending upon the nature of the external force the system can leave the equilibrium state and exhibit new dynamics: the system may have oscillatory (periodic or quasi-periodic) behaviour or show an even more complicated time evolution, characterised by the existence of *strange attractors* [13], i.e. subsets of the phase space of the system to which orbits are attracted and on which nearby trajectories display exponential divergence (on the average). An interesting question is how these attractors arise as some parameter of the system is varied, and to what degree they are dependent on the driving parameter. Several routes to chaos have now been well documented; these include infinite period-doubling cascades, intermittency and sharp transitions from a periodic or quasi-periodic regime to a chaotic one. Sudden qualitative changes, called *crises*, have been observed numerically and may also cause a transition to chaos. If a system is characterised by only one parameter, it is relatively easy to study the routes to chaos as the parameter is varied. For real physical systems, however, the number of parameters is usually larger than one: even simple systems such as nonlinear oscillators which are externally driven, have, apart from their natural frequency, the driving frequency and the damping coefficient as important parameters. Nevertheless, in many cases a typical picture can be obtained if all the parameters are kept fixed and only the amplitude of the driving force, for example, is varied.

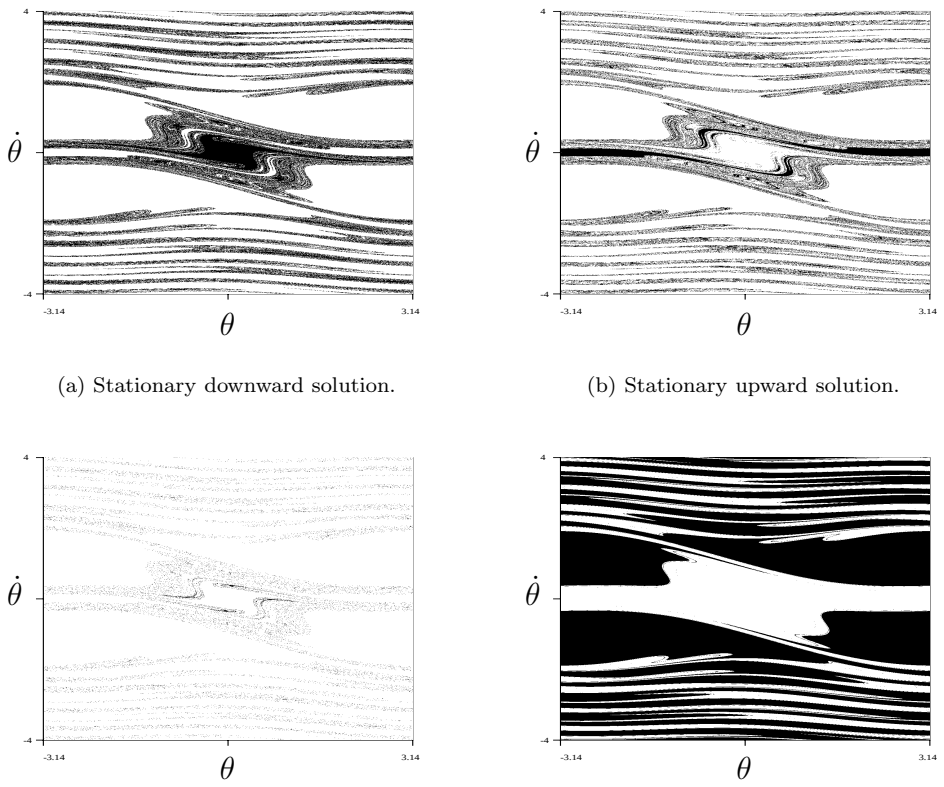

(a) Stationary downward solution.

(b) Stationary upward solution.

(c) Oscillating solution.

(d) Running solutions.

Figure 10: Coexistence of five basins of attraction (in black) for the vertically driven pendulum with $\alpha = 0.02$, $\beta = 0.35$ and $\gamma = 0.03$.

In this section we analyse the dynamics of our system by fixing α (and γ, so that, for the linearized equation obtained from (2.7) one has a fixed value $\alpha' = \alpha - \gamma^2/4$; see Sect. 2) and by scanning values of β along a vertical line in the plane (α, β).

For α and γ, we choose the values $\alpha = 0.5$ and $\gamma = 0.03$. From the stability diagram of Mathieu's equation, in Figure 2, one can see that, for the linear case with $\gamma = 0$, see (2.5), the critical value of β for the stability of the downward state is 0.6058. For the full system (2.7) one finds numerically for the critical value $\beta_c = 0.6063$; above β_c the stationary downward state for the linear system is unstable. For $\beta \geq 0.55$ a period doubling transition to chaos occurs when the parameter β increases. We have detected up to 32–period. More precisely for $\beta \in (0, 0.55)$ a period one occurs; at $\beta = 0.55$, $\beta = 0.618$, $\beta = 0.6352$, $\beta = 0.6391$, $\beta = 0.6401$ period doubling bifurcations occur, leading to orbits with period 2, 4, 8, 16, 32, respectively. For β larger than $\beta_d = 0.64018$ the motion is fully chaotic.

We computed some Poincaré sections (or stroboscopic phase representations, see below) [27, 28, 32, 33] using the full equation (2.7) and choosing $\beta = 0.7$. A typical picture is shown in Figure 11b, which gives the evolution of 1600 initial conditions (disregarding the first few iterates): we think that it represents a strange attractor, because the flow has a positive Lyapunov exponent as we show in Sect. 5 below. Analogous pictures have been found numerically also for similar models [9, 12, 32, 39]. By proceeding as in Sect. 3, we found numerical evidence that such an attractor be the only attractor in that regime.

Note that, even if the strange attractor disappears below β_c, there are still initial conditions whose first iterates appear as a sequence of dots lying over the remnant of the strange attractor existing above β_c before being swept towards some of the attractors, according to the scenario described by Blackburn, Smith and Edmundson in similar systems [9]. This is shown in Figure 12.

As we cross the critical line from above the system shows an oscillatory behaviour. Keeping α and γ the same parameter values, namely $\alpha = 0.5$ and $\gamma = 0.03$, and setting $\beta = 0.63$ we found that the system behaves periodically: the Poincaré sections consist of four dots which show that the

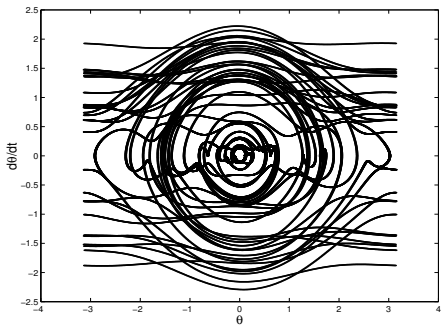

(a) Chaotic trajectory with initial datum $(\theta, \dot{\theta}) = (0.1,0)$.

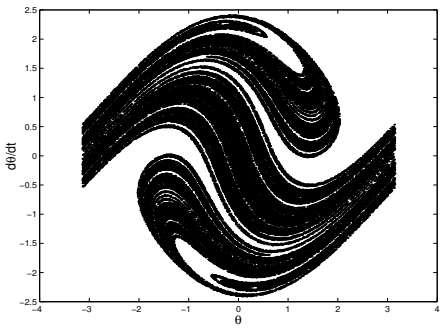

(b) Poincaré section with sampling phase shift of 3 (in radians).

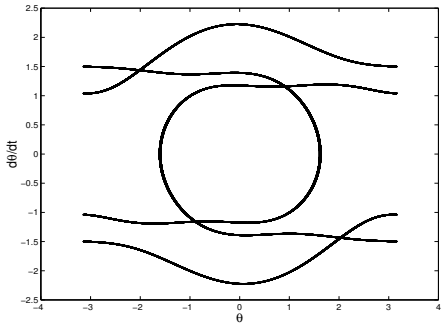

(c) Periodic orbit with period 4 with initial datum $(\theta, \dot{\theta}) = (0.1, 0)$.

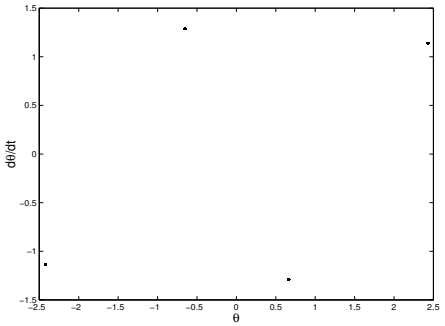

(d) Poincaré section with sampling phase shift of 1 (in radians).

Figure 11: A chaotic trajectory and a periodic trajectory with the corresponding Poincaré sections for $\alpha = 0.5$ and $\gamma = 0.03$. The values of β are respectively $\beta = 0.70$ and $\beta = 0.63$. Transients are disregarded.

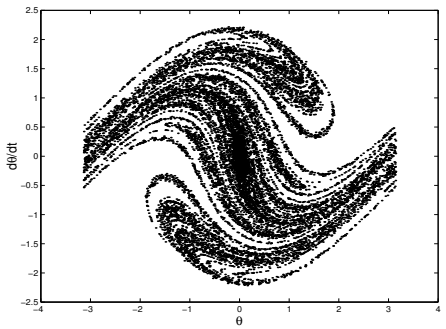

(a) Strange attractor remnant for $\alpha = 0.5$, $\beta = 0.5$ and $\gamma = 0.03$.

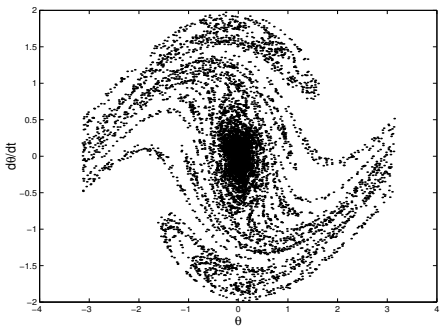

(b) Strange attractor remnant for $\alpha = 0.5$, $\beta = 0.3$ and $\gamma = 0.03$.

Figure 12: Strange attractor remnants for $\alpha = 0.5$ and $\gamma = 0.03$.

system is tending toward an orbit on which the motion is periodic with period 4 (see above).

To generate the pictures in Figure 11b,d we have computed the Poincaré sections obtained by removing one of the phase space dimensions (in our case the time 'τ'). The key point is that this simplified geometry nevertheless contains the essential information about the possible chaoticity of

the system's dynamics. Since our system has a natural period associated with it, i.e. the period of the forcing term, then the plane of the Poincaré sections could be a surface corresponding to a definite but arbitrarily chosen phase of that forcing (so in our case Poincaré sections and stroboscopic phase representations can be identified [13]). The choise of the plane is not crucial as long as the trajectories cut the surface transversally, that is the trajectories do not run parallel or almost parallel to the surface as they pass through. In our case the Poincaré sections are formed by recording the values of the angle, and the corresponding angular velocity whenever the phase of the periodic force reaches some definite value. The pictures qualitatively do not change if the sampling phase shift is fixed to other values, with respect to the ones explicitly considered in the Figures.

Similar results are obtained along the scan line β for $\alpha = -0.1$ and $\gamma = 0.08$. For the linear undamped system (2.6) the critical value for stability is $\beta = 0.618$.

For values of β less than $\beta_d = 2.145$ the system have an oscillatory behaviour; depending on the value of β trajectories will eventually end up to a smooth attractor as shown in Figure 13.

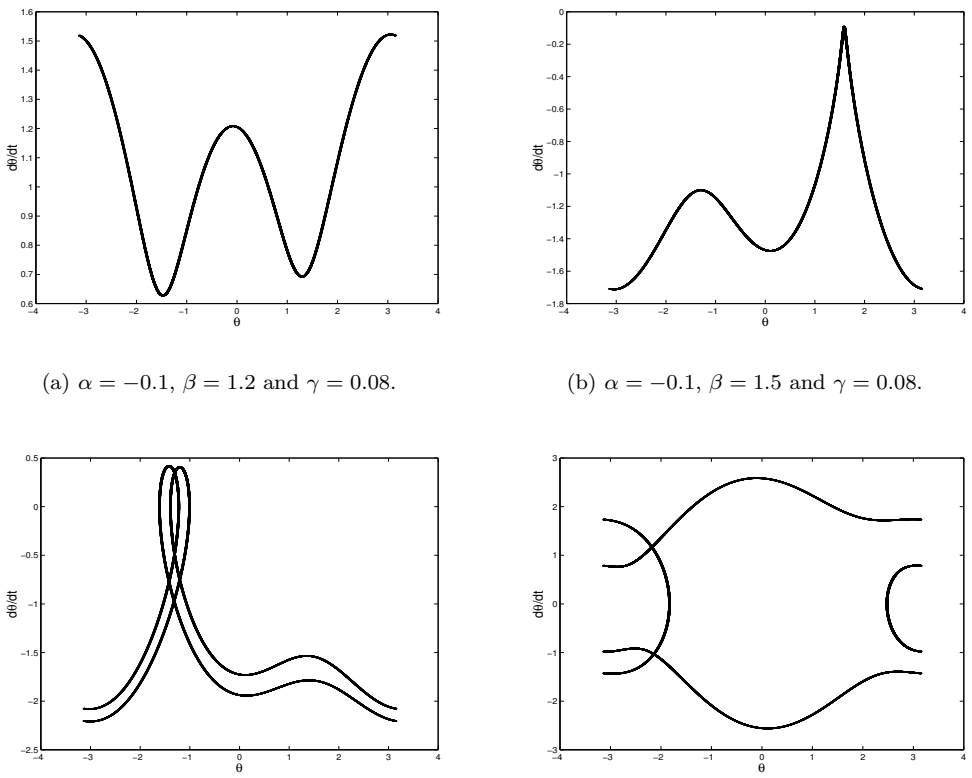

(a) $\alpha = -0.1$, $\beta = 1.2$ and $\gamma = 0.08$.

(b) $\alpha = -0.1$, $\beta = 1.5$ and $\gamma = 0.08$.

(c) $\alpha = -0.1$, $\beta = 1.8$ and $\gamma = 0.08$;

(d) $\alpha = -0.1$, $\beta = 2.1$ and $\gamma = 0.08$.

Figure 13: Smooth attractors (disregarding transients) for $\alpha = -0.1$ and $\gamma = 0.08$.

The upward state becomes unstable at $\beta_c = 0.623$: then one has a Hopf bifurcation leading to a *flutter mode* [8]: for $\beta_c < \beta < \beta_e = 0.679$ the pendulum oscillates around the vertical at half the drive frequency with an amplitude which increases as $\beta - \beta_c$; see Figure 14 a. By further increasing β the oscillating orbit disappears and only rotating attractors are left, up to the value β_d: again this is in agreement with the results found by Blackburn, Smith and Grønbech-Jensen exactly for the same model [8]. For β taking values larger than the value of $\beta_d = 2.145$ the motion is chaotic, as shown in Figure 14b.

5 Lyapunov exponents and sensitivity to initial conditions

As we mentioned in Sect. 4, our system can exhibit regular periodic motions as well as complicated non-periodic motions. Although there is a lack of mathematical proofs, a lot of numerical investig-

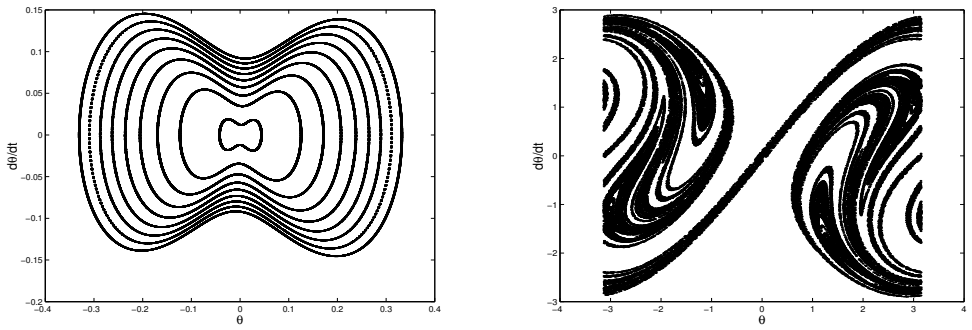

(a) (b)

Figure 14: (a) Oscillating attractors corresponding to the flutter mode for $\alpha = -0.1$ and $\gamma = 0.08$, at different values of $\beta \in (0.623, 0.679)$. (b) Poincaré section for $\alpha = -0.1$, $\beta = 2.2$ and $\gamma = 0.08$, with sampling phase shift of 1 (in radians) of a chaotic trajectory; 1600 orbits as shown (disregarding transients).

ations and some experiments on physical systems have yielded evidence that stable chaotic motions really exist for certain parameter intervals. The assumptions concerning the chaotic motions are supported by approximate values for quantities characterizing the chaos, i.e. entropies, fractal dimensions, Lyapunov exponents. One of the fundamental characteristic of a chaotic physical system is its sensitivity to the initial state. By sensitivity to initial conditions we mean that if two identical mechanical systems are started at initial conditions $\boldsymbol{x}$ and $\boldsymbol{x} + \boldsymbol{\epsilon}$ respectively, where $\boldsymbol{\epsilon}$ is a very small quantity, their dynamical states will diverge from each other very quickly in phase space, their separation increasing exponentially on the average.

Lyapunov exponents (often written as λ) play an important role in the theory of both dissipative and non-dissipative systems. They provide a computable, quantitative measure of divergence of two initially nearby trajectories. If two nearby trajectories on a chaotic attractor start off with a separation d_0 at time $t = 0$, then the trajectories diverge so that their separation at time t, denoted by $d(t)$, satisfies the expression $d(t) \approx d_0 e^{\lambda t}$ [13].

We study here the time evolution of equation (2.7) by using Lyapunov exponents; we numerically show that for some parameters values, we have positive Lyapunov exponents, thus confirming the chaotic character of the motion. For a dissipative system the sum of the exponents must be negative. If the system is chaotic then at least one of the exponents is positive. For our system there are two Lyapunov exponents corresponding to the two dimensions of the phase space $(\theta, \dot{\theta})$. In Sect. 4, we have proposed that the Poincaré section in Figures (11b, 14b) represents a strange attractor. We have computed the largest Lyapunov exponent (which is obtained from the linearization of system (2.7)) for the same parameters values we chose to obtain Figures 11b and 14b. We found that for $\alpha = 0.5$, $\beta = 0.7$ and $\gamma = 0.03$ the Lyapunov exponent settles down to 0.179563, while for $\alpha = -0.1$, $\beta = 2.2$ and $\gamma = 0.08$ the Lyapunov exponent settles down to 0.207936. For both cases the number of time steps was 10^7 with time unit set at 0.001. The above results are a true indicator of the chaotic behaviour of the system. In Table 1 we give a list of some computed Lyapunov exponents as β is varied. We should note here that in the chaotic regime the Lyaponov exponent is related with any initial condition that tends to the only existing attractor (i.e. Figures 11b or 14b). In the non chaotic regime, the Lyapunov exponent is related with any initial condition that tends to one of the rotating attractors found in Sect 3 and 4 .

6 An analytical proof of asymptotic stability

In the following, with respect to the previous sections, we are slightly changing the notations, in order to make more terse the comparison with the existent mathematical literature on the subject, especially with [5] and [10].

If we are interested in the stability of the position $\theta = \pi$ (upside-down pendulum), define $\xi = \pi + \theta$,

β	Lyapunov exponents λ
0.63	-0.0140605
0.64	-0.0143172
0.64018	0.0109093
0.64019	0.141205
0.65	0.179953
0.67	0.180256
0.68	0.178863
0.69	0.179888
0.70	0.179563

β	Lyapunov exponents λ
0.8	-0.0399938
0.9	-0.0399802
1.3	-0.039983
1.6	-0.0399905
1.9	-0.0399149
2.14	-0.0395598
2.145	0.0242153
2.2	0.207936
2.5	0.228123

Table 1: Computed Lyapunov exponents as β is varied ; the left table corresponds to values of $\alpha = 0.5, \gamma = 0.03$, while the right table correponds to values of $\alpha = -0.1, \gamma = 0.08$.

so that (2.7) becomes

$$\ddot{\xi} + \sin\xi \left(-\frac{g}{\ell} + \frac{b\omega^2}{\ell} \cos\omega t \right) + \gamma\, \dot{\xi} = 0. \tag{6.1}$$

Define $\omega t = 2\tau$ and $x(\tau) = \xi(t)$; then (6.1) writes

$$\ddot{x} + \sin x\, (a + 2q\cos 2\tau) + 2\lambda \dot{x} = 0, \qquad a = -\frac{4g}{\ell\omega^2}, \qquad q = \frac{2b}{\ell}, \qquad \lambda = \frac{\gamma}{\omega}, \tag{6.2}$$

(with $\dot{x} = \mathrm{d}x/\mathrm{d}\tau$ and $\ddot{x} = \mathrm{d}^2x/\mathrm{d}\tau^2$), which can be rewritten as

$$\ddot{x} + f(\tau)\, x + 2\lambda\dot{x} = [x - \sin x]\, f(\tau), \qquad f(\tau) = a + 2q\cos 2\tau. \tag{6.3}$$

Set

$$x(\tau) = \delta e^{-\lambda\tau} y(\tau) \ : \tag{6.4}$$

then, by writing (6.3) with $\sin x$ expressed as Taylor series of x and dividing it by $\delta\, e^{-\lambda\tau}$, we obtain

$$\ddot{y} + f_0(\tau)\, y = f(\tau) \sum_{m=1}^{\infty} \frac{(-1)^{m+1}}{(2m+1)!}\, e^{-2m\lambda\tau} \varepsilon^m y^{2m+1}, \qquad \varepsilon = \delta^2, \tag{6.5}$$

where

$$f_0(\tau) = f(\tau) - \lambda^2 = a_0 + 2q\cos 2\tau\ , \qquad a_0 = a - \lambda^2\, . \tag{6.6}$$

In the linear case ($\varepsilon = 0$) the substitution (6.4) is the standard procedure to show that the solutions of Mathieu's equation with damping are conjugated to the solutions of Mathieu's equation; see Sect. 2.

For $\varepsilon = 0$, (6.5) becomes (the standard form of) Mathieu's equation,

$$\ddot{y} + f_0(\tau)\, y = 0\, , \qquad f_0(\tau) = a_0 + 2q\cos 2\tau\, ; \tag{6.7}$$

we refer to [24], Ch. 8, for an introductory review and to [5] for a more detailed exposition of the subject.

Note that in (6.6) one has $a_0 < 0$ (see (6.2) and (6.6)). Let $a_0(q)$, $b_1(q)$ be the curves of the first *characteristic values* of Mathieu's equation, [5], Ch. III; for a_0, q such that $a_0(q) < a_0 < \min\{b_1(q), 0\}$ the solution of 6.7 is stable, [5], Ch. VI. More precisely there exist two independent (Floquet) solutions

$$u_1(\tau) = e^{i\mu_0\tau} p_0(\tau)\, , \qquad u_2(\tau) = e^{-i\mu_0\tau} \bar{p}_0(\tau)\, , \tag{6.8}$$

where $0 < \mu_0 < 1$, [5, 10], and $p_0(\tau)$ is an analytic function of period π ,

$$p_0(\tau) = \sum_{\nu\in\mathbb{Z}} e^{2i\nu\tau} p_{0\nu}\, , \qquad p_0(0) = 1\, , \qquad p_0(-\tau) = \bar{p}_0(\tau)\, ; \tag{6.9}$$

here and henceforth, given $z \in \mathbb{C}$, $\bar{z}$ denotes the complex conjugate of z. Both μ_0 and $p_0(\tau)$ depend on a_0 and q. Note that

$$|p_{0\nu}| \leq P\, e^{-\kappa|\nu|}, \qquad P = \max_{\tau\in[0,\pi]} |p_0(\tau)|\,, \tag{6.10}$$

for some $\kappa \in \mathbb{R}_+$.

One can construct two real independent solutions as

$$w_1(\tau) = \frac{1}{2}\left[e^{i\mu_0\tau}p_0(\tau) + e^{-i\mu_0\tau}\bar{p}_0(\tau)\right], \qquad w_2(\tau) = \frac{1}{2ic}\left[e^{i\mu_0\tau}p_0(\tau) - e^{-i\mu_0\tau}\bar{p}_0(\tau)\right], \tag{6.11}$$

where $c \in \mathbb{R}$ is such that $\dot{w}_2(0) = 1$. Note that w_1 is even and w_2 is odd.

The solution $y^{(0)}(\tau)$ of (6.7) with initial data $(y^{(0)}(0), \dot{y}^{(0)}(0)) = (A, B) \in \mathbb{R}^2$ can be written as

$$y^{(0)}(\tau) = w_1(\tau)\, A + w_2(\tau)\, B, \qquad A^2 + B^2 = 1, \tag{6.12}$$

hence it is in general quasi-periodic (periodic if μ_0 is rational), with *rotation vector* $\omega_0 = (\mu_0, 2)$. The normalization condition in (6.12) is imposed just for convenience; see (6.16) below.

In terms of the Floquet solutions, (6.12) becomes

$$y^{(0)}(\tau) = u_1(\tau)\, C + u_2(\tau)\, D = e^{i\mu_0\tau}p_0(\tau)\, C + e^{-i\mu_0\tau}\bar{p}_0(\tau)\, D, \tag{6.13}$$

where

$$C = \frac{A - iB/c}{2}, \qquad D = \bar{C} = \frac{A + iB/c}{2}. \tag{6.14}$$

Expressed in the variable x, the solution $y^{(0)}$ becomes

$$x^{(0)}(\tau) \equiv \delta e^{-\lambda\tau} y^{(0)}(\tau) = \delta\left[e^{i\mu_0\tau - \lambda\tau}p_0(\tau)\, C + e^{-i\mu_0\tau-\lambda\tau}\bar{p}_0(\tau)\, D\right], \tag{6.15}$$

so that one sees that its limit for $\tau \to \infty$ tends to 0: if one neglects the nonlinear terms in (6.3) the origin is asymptotically stable. Note that, in terms of the variable x, the initial condition in (6.12) gives

$$x^{(0)2}(0) + \dot{x}^{(0)2} = \delta^2, \tag{6.16}$$

so that δ measures the distance of the initial datum from the equilibrium point $(0, 0)$.

The solution $x^{(0)}$ given by (6.15) can be written as

$$x^{(0)}(\tau) = \sum_{\nu\in\mathbb{Z}^2} e^{i\omega_0\cdot\nu\tau - 2\lambda\tau} x^{(0)}_\nu, \tag{6.17}$$

where $\omega_0 = (\mu_0, 2)$, $\nu = (\nu_1, \nu_2)$, with $\nu_1 = \pm 1$ and $x^{(0)}_{(1,\nu_2)} = \bar{x}^{(0)}_{-(1,\nu_2)} = \delta p_{0,\nu_2} C$; here and henceforth $\cdot$ denotes the inner product in $\mathbb{Z}^2$, so that $\omega_0 \cdot \nu = \mu_0\nu_1 + 2\nu_2$. Hence $x^{(0)}(\tau)$ depends on τ only through $e^{\pm i\mu_0\tau}$, $e^{\pm i2\tau}$ and $e^{-\lambda\tau}$. The first factors gives an oscillatory behaviour, while the third one is responsible for the decay towards the origin.

If $\varepsilon \neq 0$ we look for solutions analytic on ε for ε small enough, whose dependence on τ is still through the factors $e^{\pm i\mu_0\tau}$, $e^{\pm i2\tau}$ and $e^{-\lambda\tau}$. This means that we look for solutions of the form

$$y(\tau) \equiv y(\tau;\varepsilon) = \sum_{n=1}^{\infty} \varepsilon^n y^{(n)}(\tau) = \sum_{n=1}^{\infty} \varepsilon^n \sum_{\nu\in\mathbb{Z}^2}\sum_{k=0}^{\infty} e^{i\omega_0\cdot\nu\tau - k\lambda\tau} y^{(n)}_{\nu,k}. \tag{6.18}$$

We shall show that, fixed an arbitrary direction (A, B), with $A^2 + B^2 = 1$, in the plane $(y, \dot{y})$, the solution $y(\tau)$ of (6.5), with initial condition $(y(0), \dot{y}(0)) = (y^{(0)}(0), \dot{y}^{(0)}(0)) = (A, B)$, remains bounded around the equilibrium point $(0, 0)$, provided ε is small enough. Note that the component $k = 0$ already appears when $n = 0$, i.e. for $y^{(0)}(\tau)$: anyway the presence of oscillating (or even constants, that is with $k = 0$ and $\nu = 0$) terms is not a problem because the solution $x(\tau)$ of the equation (6.3) is related to $y(\tau)$ through the change of variable (6.4), and $\theta(t)$ is such that $x(\omega t/2) = \pi + \theta(t)$.

Then $(x(0), \dot{x}(0)) = (\delta A, \delta B)$ is the initial datum for the equation (6.3), hence $(\theta(0), \dot{\theta}(0)) = (\pi + \delta A, \delta B)$ is the initial datum for the equation (2.7). By the above discussion we have that any initial datum near enough to the equilibrium point $(\pi, 0)$ generates a solution of (2.7) which is

exponentially asymptotic to $(\pi, 0)$: this implies the asymptotic stability of the position $(\theta, \dot{\theta}) = (\pi, 0)$ for the upside-down pendulum.

More formally the result can be stated as follows.

THEOREM. *Given the equation (2.7), assume that the parameters ω and b are such that*

$$a_0(2b/\ell) < -\frac{4g}{\ell\omega^2} - \lambda^2 < \min\{b_1(2b/\ell), 0\}\,, \tag{6.19}$$

where $q \to a_0(q)$ and $q \to b_1(q)$ are the curves of the first characteristic values of Mathieu's equation. Then the series (6.18) is absolutely convergent for ε small enough. This means that there exists $\delta_0 > 0$ such that the equilibrium position $(\theta, \dot{\theta}) = (\pi, 0)$ is the ω-limit set of any initial datum $(\theta(0), \dot{\theta}(0))$ satisfying $[\theta(0) - \pi]^2 + \dot{\theta}^2(0) < \delta_0^2$. In particular the ball of center $(\pi, 0)$ and radius δ_0 is contained inside the basin of attraction of $(\pi, 0)$; one has $\delta_0 = O(\sqrt{\lambda})$.

The proof of the above Theorem is carried out in Appendix A. The condition (6.19) could be easily relaxed into a weaker one. In fact (6.18) requires the solution $y^{(0)}$ to be quasi-periodic: in terms of the parameters ω, b this means that they lay inside the lowest stability region, so that μ_0 is real, [5]. Anyway the solution $x^{(0)}$ has a damping factor $e^{-\lambda\tau}$ (see (6.15)), so that μ_0 could be allowed to have also an imaginary part (smaller than λ). As we are not looking for optimal bounds, we have neglected such a feature in stating the Theorem; however recall that the damping term destabilizes the motion of the inverted pendulum with respect to the undamped case [30].

Using that $a_0(q) \approx 1 - q^2/2$ for q small enough, for $\lambda = 0$ the condition (6.19), if $b/\ell \leq 0.450$ so that $\min\{b_1(2b/\ell), 0\} = 0$, reads as $2g\ell < b^2\omega^2$, which is the condition found by the averaging method (see [36], Ch. 9; compare also [1], formula (2.1), for a single pendulum).

The analytical result stated by the Theorem can also be checked using a computer animation. To accomplish this, we have created a Maple program which numerically integrate the equation of motion (6.1), with parameters values $b = 0.35$, $\ell = 1$, $\omega = 10$ and $g = 1$. For the purpose of the illustration we chose a large value of the dissipative parameter, $\gamma = 0.99$: such a value enables us to achieve the Figure 15, with initial conditions $(\theta, \dot{\theta}) = (2.7, 0)$, within 56 time-steps. As we expect, due to dissipation, the oscillation of the pendulum and the initial phase point terminates at $(\pi, 0)$, which is the fixed point; however the pendulum is still moving up and down because there is some energy left due to the forcing. A second order symplectic integration routine was used.

We note also the theorem above (more exactly the convergence of the series (6.18) and the definition of the change of variables (6.4)) implies that the solutions $\theta(t)$, with initial conditions inside the basin of attraction of $(\theta, \dot{\theta}) = (\pi, 0)$ converge to such point exponentially, at a rate which, in terms of (6.2) reads as λ. The numerical computation of the largest Lyapunov exponent λ for the upward state, at the fixed values of the parameters, gives the value λ, in excellent agreement with the results found analtycally.

In our analytical estimates no optimality has been looked for. Note that our bounds work for any kind of perturbation with respect to the linear case, (we simply show in the Appendix A that the nonlinear terms do not worsen the conditions of stability holding in the linear case), so they do not distinguish between an interaction $\cos\theta$ (as the vertically driven pendulum yields) and, for instance, an interaction $\cosh\theta$: of course in the first case a larger basin of attraction is expected. Note also that we explicitly use the parity of the perturbation in order to obtain an expansion in powers of $\varepsilon = \delta^2$ (see Appendix A): however this is not at all an essential feature, and the analysis can be easily adapted to any kind of analytic perturbation (simply expanding directly in powers of δ). It would be interesting to try to take advantage of the exact form of the interaction in order to improve the bounds: as a matter of fact the nonlinear terms could even improve such conditions, and this is what likely happens physically. For the reason explained above the bounds of the stability regions (in phase space) are far worse than the experimentally observable ones [4].

The bound on the diameter of the basin of attraction given by the Theorem is not uniform in λ (it shrinks to zero for $\lambda \to 0$). On the other hand, in absence of friction, the equilibrium position $(\pi, 0)$ is expected to be stable for ω large enough, see Sect. 2. Within the linear approximation a bound of the stability region in the plane (a, q) is given in [1]. If one wants to take into account also the nonlinear terms, one can use KAM type arguments to prove rigorously the stability for the undamped pendulum [7].

In absence of friction no stability is in general expected in the case of more than one pendulum. The existence of KAM tori (which could be easily proved also in such a case) is no more sufficient to

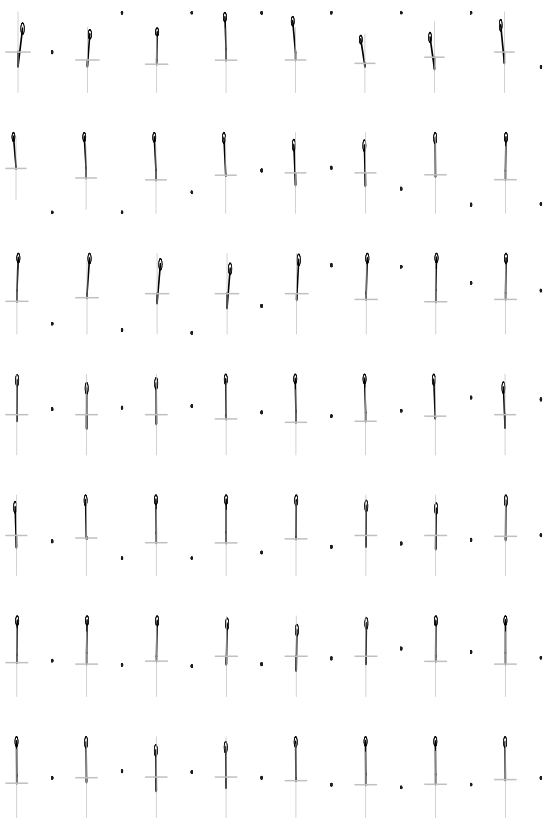

Figure 15: An illustation of the effect of dissipation in the vertically driven pendulum using a computer animation. Each pendulum is equivalent to 1 time-step. The dot in each picture corresponds to the position of the phase point of the orbit (the phase plane coincides with the plane of the pendulum).

prevent *Arnol'd diffusion*. Anyway one could probably prove stability on long times (of Nekhoroshev type), for instance by following the methods in [18].

7 Concluding Remarks

In this paper we investigated a planar pendulum with parametric vertical time-periodic forcing. Analytical and numerical techniques were employed to analyse the various dynamical features of the system.

First we studied the linearised system, described by Mathieu's equation. We have shown numerically that the solutions of the linearised system, for various values of the parameters α and β near the two equilibrium states can be either stable or unstable in accordance with the well known theory of Mathieu's equation.

Then the attractors and their associated basins of attraction were computed for the upward and downward state of the pendulum. We found that for those values of the parameters such that the two equilibrium states are stable, there is a coexistence of four different attractors for the downward state and three different attractors for the upward state of the pendulum. Depending on the initial conditions, trajectories converge towards one of these attractors.

Additionally, we showed numerically that these are the only attractors for the downward and upward position of the pendulum. These results are very important and significantly contribute towards having a more complete picture of the dynamics of this system.

Furthermore Poincaré sections, phase portraits and sensitivity to initial condiltions provide information about the dynamics of the pendulum for specific values of the parameters α, β and δ. We

found that depending on the values of α and β the pendulum can show an oscillatory behaviour or an even more complicated time evolution, characterized by the existence of strange attractors. We have strengthened this scenario by computing the Lyapunov exponents, which they turn out to be positive as they should.

Finally, an analytical proof of asymptotic stability was developed; we have rigorously shown that in the presence of small dissipation, the upward equilibrium position becomes asymptotically stable. This result is in excellent agreement with numerical computations, advanced visualization techniques and real experiments [4].

A Proof of the Theorem

We look for solutions of the form

$$y(\tau) \equiv y(\tau;\varepsilon) = \sum_{n=1}^{\infty} \varepsilon^n y^{(n)}(\tau). \tag{A.1}$$

Inserting (A.1) into (6.5), we obtain, by equating the terms of the same order in ε,

$$\begin{aligned} \ddot{y}^{(0)} + f_0(\tau)\, y^{(0)} &= 0\,, \\ \ddot{y}^{(1)} + f_0(\tau)\, y^{(1)} &= \frac{1}{3!} e^{-2\lambda\tau} f(\tau) y^{(0)3}\,, \\ \ddot{y}^{(2)} + f_0(\tau)\, y^{(2)} &= \frac{1}{2} e^{-2\lambda\tau} f(\tau)\, y^{(0)2} y^{(1)} - \frac{1}{5!} e^{-4\lambda\tau} f(\tau)\, y^{(0)5}\,, \end{aligned} \tag{A.2}$$

and so on; in general, to order n, one has

$$\ddot{y}^{(n)} + f_0(\tau)\, y^{(n)} = F^{(n)}(\tau), \tag{A.3}$$

where

$$\begin{aligned} F^{(n)}(\tau) &= f(\tau) \sum_{m=1}^{n} \frac{(-1)^{m+1}}{(2m+1)!} e^{-2m\lambda\tau} \sum_{m'=0}^{2m+1} \binom{2m+1}{m'} y^{(0)2m+1-m'}(\tau) \\ &\qquad \sum_{\substack{n_1\geq 1,\ldots,n_{m'}\geq 1 \\ n_1+\ldots+n_{m'}=n-m}} \prod_{j=1}^{m'} y^{(n_j)}(\tau). \end{aligned} \tag{A.4}$$

The term corresponding to $m' = 1$ yields $m = n$ and it has to be interpreted as

$$f(\tau) \frac{(-1)^{n+1}}{(2n+1)!} e^{-2n\lambda\tau} y^{(0)2n+1}(\tau); \tag{A.5}$$

note that for $n = 1$ it is the only present (see (A.2).

Then the equations (A.3) can be iterarively integrated as

$$\begin{pmatrix} y^{(n)}(\tau) \\ \dot{y}^{(n)}(\tau) \end{pmatrix} = W(\tau) \left[\begin{pmatrix} y^{(n)}(0) \\ \dot{y}^{(n)}(0) \end{pmatrix} + \int_0^\tau \mathrm{d}\tau'\, W^{-1}(\tau') \begin{pmatrix} 0 \\ F^{(n)}(\tau') \end{pmatrix} \right], \tag{A.6}$$

where

$$W(\tau) = \begin{pmatrix} w_1(\tau) & w_2(\tau) \\ \dot{w}_1(\tau) & \dot{w}_2(\tau) \end{pmatrix} \tag{A.7}$$

is the Wronskian matrix of the linear system (6.7), so that $W(0) = \mathrm{id}$ and $\det W(\tau) = 1$.

Introduce the space $\mathcal{M}$ of functions $h\colon \mathrm{R} \to \mathrm{C}$, which admit a formal expansion of the form

$$h(\tau) = \sum_{\nu\in\mathbb{Z}^2} \sum_{k=0}^{\infty} e^{i\nu\cdot\omega_0\tau} e^{-k\lambda\tau} h_{\nu,k} \tag{A.8}$$

and define

$$\mathcal{M}_0 = \{h \in \mathcal{M} \ : \ h_{0,0} = 0\}. \tag{A.9}$$

Note that

$$\int_0^\tau \mathrm{d}\tau' \left[e^{i\omega_0\cdot\nu\tau' - k\lambda\tau'}\right] = \frac{e^{i\omega_0\cdot\nu\tau - k\lambda\tau} - 1}{i\omega_0\cdot\nu - k\lambda} \tag{A.10}$$

for all $(\nu, k) \in \mathrm{Z}^2 \times \mathrm{N}$.

Given a function $h \in \mathcal{M}_0$ denote by $\mathcal{I}(h)$ the primitive of h in $\mathcal{M}_0$: then, by (A.10), one can see that

$$\mathcal{I}\left[e^{i\omega_0\cdot\nu\tau' - k\lambda\tau'}\right] = \frac{e^{i\omega_0\cdot\nu\tau - k\lambda\tau}}{i\omega_0\cdot\nu - k\lambda}, \tag{A.11}$$

as $h \in \mathcal{M}_0$ requires $h_{\nu,k}$ to have $(\nu, k) \neq (0, 0)$. The space $\mathcal{M}$ admits a natural decomposition into

$$\mathcal{M} = \bigoplus_{\nu\in Q}\bigoplus_{k=1}^{\infty} \mathcal{M}_{\nu,k}, \qquad Q = \{\nu \in \mathrm{Z}^2 \ : \ \nu \sim \nu' \text{ if } \omega_0\cdot\nu = \omega_0\cdot\nu'\}, \tag{A.12}$$

and $\mathcal{M}_{\nu,k}$ is the space of functions of the form $h(\tau) = a\, e^{i\omega_0\cdot\nu'\tau}e^{-k\lambda\tau}$, with $a \in \mathrm{C}$ and for all ν' in the same equivalence class of ν. Note that $Q = \mathrm{Z}^2$ if the components of ω_0 are rationally independent. By construction $\mathcal{I}\colon \mathcal{M}_{\nu,k} \to \mathcal{M}_{\nu,k}$.

Define the function w_{12} as

$$w_{12}(\tau,\tau') = [w_2(\tau)w_1(\tau') - w_1(\tau)w_2(\tau')] = \frac{1}{2ic}\left[u_1(\tau)u_2(\tau') - u_2(\tau)u_1(\tau')\right]. \tag{A.13}$$

One can write explicitly (A.6) as

$$\begin{aligned}\begin{pmatrix} y^{(n)}(\tau) \\ \dot y^{(n)}(\tau)\end{pmatrix} \ &= \ \begin{pmatrix} w_1 y^{(n)}(0) + w_2\dot y^{(n)}(0) \\ \dot w_1 y^{(n)}(0) + \dot w_2\dot y^{(n)}(0)\end{pmatrix} \\ &\quad + \int_0^\tau \mathrm{d}\tau' \begin{pmatrix} [w_2(\tau)w_1(\tau') - w_1(\tau)w_2(\tau')]\, F^{(n)}(\tau') \\ [\dot w_2(\tau)w_1(\tau') - \dot w_1(\tau)w_2(\tau')]\, F^{(n)}(\tau')\end{pmatrix}.\end{aligned} \tag{A.14}$$

Choose (for simplicity) initial data such that $(y^{(n)}(0), \dot y^{(n)}(0)) = (0, 0)$: this means that the initial datum remains $(y(0;\varepsilon), \dot y(0;\varepsilon)) = (y^{(0)}(0), \dot y^{(0)}(0)) = (A, B)$ for all ε for which the solution $y(\tau;\varepsilon)$ is defined.

Then (A.14) gives for the first component

$$y^{(n)}(\tau) = \int_0^\tau \mathrm{d}\tau'\, w_{12}(\tau,\tau')\, F^{(n)}(\tau') == \mathcal{I}\left(w_{12}F^{(n)}\right)(\tau) - \mathcal{I}\left(w_{12}F^{(n)}\right)(0). \tag{A.15}$$

In particular one has

$$y^{(1)}(\tau) = \sum_{\sigma=0,1} \mathcal{I}\left(\frac{1}{3!}w_{12}(\tau,\tau')e^{-2\lambda\tau'}f(\tau')y^{(0)3}(\tau')\right)(\sigma\tau), \tag{A.16}$$

for the first order term; see (A.2).

By expressing $y^{(n)}$ as in (A.15) and developing $F^{(n)}$ as in (A.4), one obtains an (integral) expression of $y^{(n)}$ in terms of functions $y^{(n')}$, with $n' < n$. One can iterate the procedure until only terms $y^{(1)}$ given by (A.16) appear. In such a way one is naturally led to represent $y^{(n)}$ in terms of tree graphs (or simply *trees*): we refer to [19] for an introduction to the theory of graphs.

A tree θ is a partially ordered set of points and lines connecting the points. The partial ordering is from right to left and it will be denoted by $\preceq$. The leftmost point r is called the *root* of the tree, while all the other points are called *nodes* and are denoted by labels v; by the definition of the order relation one has $r \succ v$ for all vertices v. The lines are denoted by ℓ; they are all oriented towards the root. If a line ℓ connects a node v_2 to a node $v_1 \succ v_2$, we shall write $\ell = \ell_{v_2}$ and $v_2' = v_1$: we say that the line enters v_1 and exits v_2, and that v_1 is the node immediately following v_2. The line ℓ_0 entering the root is called the *root line*: if we denote by v_0 the last node of the tree, then $\ell_0 = \ell_{v_0}$. The first nodes of a tree, i.e. the nodes which do not follow any other nodes, are called the *endpoints*

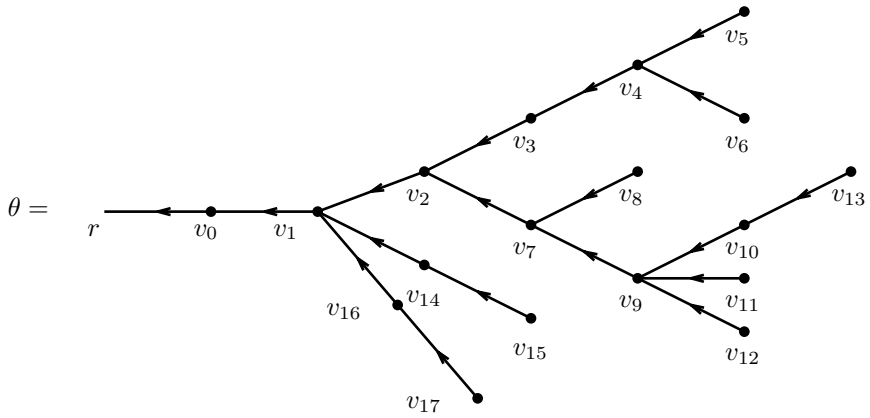

Figure 16: A tree θ with 18 nodes and 8 endpoints.

of the tree. An example of tree is given in Figure 16. We shall call $V(\theta)$ the set of nodes in θ and $\Lambda(\theta)$ the set of lines in θ: by construction $|V(\theta)| = |\Lambda(\theta)|$.

Given a tree θ and a node $v \in V(\theta)$, the set of nodes $w \preceq v$ and of lines connecting them is still a tree graph: we call it a *subtree* of θ. Its root is the node v' of θ, and its root line is the line ℓ_v, so that we can denote the subtree by θ_v, by explicitly assigning its last node (so uniquely identifying the root), and say that θ_v enters v'. By construction $\theta = \theta_{v_0}$.

If we write $y^{(0)}$ as in (6.12) we can expand in (A.4)

$$y^{(0)2m+1-m'}(\tau) = \sum_{m_1=1}^{2m+1-m'} \binom{2m+1-m'}{m_1} (w_1(\tau)A)^{m_1} (w_2(\tau)B)^{2m+1-m'-m_1} . \tag{A.17}$$

To each node we associate the labels m_v, m_{v1}, m_{v2} and m_{v3}, which are positive integers satisfying the constraint that

$$m_{v1} + m_{v2} + m_{v3} = 2m_v + 1. \tag{A.18}$$

The label m_v is called the *order label*, while m_{v3} is the *branching label*: the latter denotes the number of lines entering the node v; for instance in Figure 16 one has $m_{v_1 3} = 3$, $m_{v_2 3} = 2$, $m_{v_3 3} = 1$, $m_{v_4 3} = 2$, $m_{v_5 3} = 0$ and so on.

We define the *order* n of a tree as

$$n = \sum_{v \in V(\theta)} m_v. \tag{A.19}$$

To each node v we associate also a *time variable* τ_v, a function

$$\mathcal{A}_v(\tau_v) \equiv \frac{1}{m_{v1}! m_{v2}! m_{v3}!} (-1)^{m_v+1} e^{-2m_v \lambda \tau_v} \, (w_1(\tau_v)\, A)^{m_{v1}} \, (w_2(\tau_v)\, B)^{m_{v2}} , \tag{A.20}$$

a function $w_{12}(\tau_{v'}, \tau_v)$, and a label $\sigma_v \in \{0, 1\}$. To the root r we associate a time variable $\tau_r \equiv t$.

Note that one can associate the functions $w_1(\tau_{v'})$ and $w_2(\tau_{v'})$ in $w_{12}(\tau_{v'}, \tau_v)$ to the node v': in such a way to each node v we can associate a label $\delta_v \in \{1, 2\}$ and a label $\rho_v \in \{1, 2\}$, with $\rho_v + \delta_v = 3$, and write

$$w_{12}(\tau'_v, \tau_v) = \sum_{\delta_v + \rho_v = 3} (-1)^{\delta_v + 1} w_{\rho_v}(\tau_{v'})\, w_{\delta_v}(\tau_v). \tag{A.21}$$

Therefore we can associate to each node $v \in V(\theta)$ a *node function*

$$\mathcal{B}_v(\tau_v) = (-1)^{\delta_v + 1}\, w_{\delta_v}(\tau_v)\, \mathcal{A}_v(\tau_v) \prod_{w\,:\,w'=v} w_{\rho_w}(\tau_v) \tag{A.22}$$

and to the root a *root function*

$$\mathcal{B}_r(t) = \begin{cases} w_1(t) & \text{if } \delta_{v_0} = 2 \ , \\ w_2(t) & \text{if } \delta_{v_0} = 1 \ . \end{cases} \tag{A.23}$$

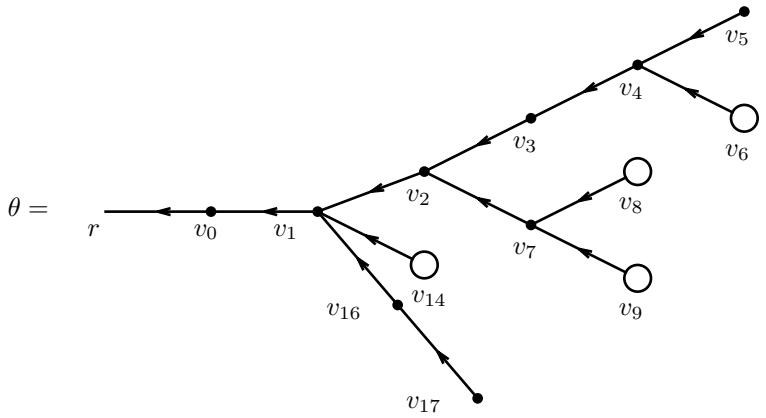

Figure 17: A reduced tree $\bar{\theta}$ with 9 free nodes and 4 leaves. It has been obtained by the tree represented in Figure 22, by encircling inside bubbles all nodes v_i with $\sigma_{v_i} = 0$, then deleting all the bubbles except the outer ones, hence representing the subtrees enclosed by the remaining bubbles as white balls. There are 6 endpoints, two of which (v_5 and v_{17}) are free nodes. One has by construction $\sigma_{v_0} = 1$, $\sigma_{v_1} = 1$, $\sigma_{v_2} = 1$, $\sigma_{v_3} = 1$, $\sigma_{v_4} = 1$, $\sigma_{v_5} = 1$, $\sigma_{v_7} = 1$, $\sigma_{v_{16}} = 1$ and $\sigma_{v_{17}} = 1$, while $\sigma_{v_6} = 0$, $\sigma_{v_8} = 0$, $\sigma_{v_9} = 0$ and $\sigma_{v_{14}} = 0$.

Finally to each node v we associate a *value* $\mathrm{Val}(\theta_v)$, which is iteratively defined as follows. For $v \prec v_0$ one sets

$$\mathrm{Val}(\theta_v) = \mathcal{I}\left(\mathcal{B}_v\right)(\tau_{v'}) - \mathcal{I}\left(\mathcal{B}_v\right)(0) = \sum_{\sigma_v = 0,1} \mathcal{I}\left(\mathcal{B}_v\right)(\sigma_v \tau_{v'}), \tag{A.24}$$

if v is an endpoint, and

$$\begin{aligned} \mathrm{Val}(\theta_v) &= \mathcal{I}\left(\mathcal{B}_v \mathrm{Val}(\theta_1) \dots \mathrm{Val}(\theta_{m_{v3}})\right)(\tau_{v'}) - \mathcal{I}\left(\mathcal{B}_v \mathrm{Val}(\theta_1) \dots \mathrm{Val}(\theta_{m_{v3}})\right)(0) \\ &= \sum_{\sigma_v = 0,1} \mathcal{I}\left(\mathcal{B}_v \mathrm{Val}(\theta_1) \dots \mathrm{Val}(\theta_{m_{v3}})\right)(\sigma_v \tau_{v'}), \end{aligned} \tag{A.25}$$

if v is not an endpoint, while for $v = v_0$ one sets

$$\mathrm{Val}(\theta) = \sum_{\sigma_{v_0} = 0,1} \mathcal{B}_r(t) \mathcal{I}\left(\mathcal{B}_{v_0} \mathrm{Val}(\theta_1) \dots \mathrm{Val}(\theta_{m_{v_0 3}})\right)(\sigma_{v_0} t). \tag{A.26}$$

Each time $\sigma_v = 0$ for some $v \in V(\theta)$ the subtree θ_v contributes a constant factor (i.e. independent of time) to the value of the tree θ: in general we have a product of several factorizing terms. This can be better understood graphically in terms of *leaves* (as done in [14], with respect to which, however, we proceed in a slightly different way). Given a tree θ, let us define the *reduced tree* $\bar{\theta}$ in the following way. For each node $v \prec v_0$ with $\sigma_v = 0$ let us draw a bubble encircling the node together with the entire subtree θ_v, and let us delete all the so obtained bubbles, but the outer ones (i.e. the "maximal bubbles"); each remaining bubble encloses a subtree with last node v and σ_v label fixed to be zero, and it becomes an endpoint v which can be graphically represented as a white ball attached to the node v' through a line ℓ_v; see Figure 17. We call *leaf* such an endpoint.

We call *free nodes* the reduced tree nodes different from the leaves; the leaves will be considered a particular type of endpoints, but they will be distinguished from the free nodes. We define the *reduced order* of a reduced tree as the sum n_0 of the labels m_v associated to its free nodes; by construction $n_0 \leq n$ (the equality holding only if there are no leaves). We can associate to a reduced tree $\bar{\theta}$ a value $\mathrm{Val}(\bar{\theta})$, where, corresponding to each free node v, there is a factor $\mathcal{B}_v$ and, corresponding to each leaf v, there is factor L_v, which will be called the *value of the leaf*: a leaf v contributes to $\mathrm{Val}(\theta)$ only through a factor $w_{\rho_v}(\tau_{v'})$ (which is taken into account in the node function $\mathcal{B}_{v'}$, see (A.22)).

Each leaf value L_v can be expressed as a tree value $\mathrm{Val}(\theta_v)$, provided that one sets $\sigma_v = 0$. The tree value $\mathrm{Val}(\theta)$ will be simply the product of the value of the reduced tree $\mathrm{Val}(\bar{\theta})$ times the values of its leaves: each leaf value L_v in turn is given by the product of the value of a reduced tree $\bar{\theta}_v$ times the product of the values of its leaves, and so on. Then in the following we can confine ourselves to

consider the case in which $\sigma_v = 1$ for all $v \in V(\theta)$, provided the nodes can be allowed to represent also leaves w contributing the functions $w_{\sigma_w}(\tau_v)$ to the value of the (reduced) tree.

If we recall the expression (A.22) for the node functions $\mathcal{B}_v$, we immediately see that each node function can be decomposed into

$$\mathcal{B}_v(\tau_v) = e^{-2m_v\lambda\tau} \sum_{\nu\in\mathbb{Z}^2} e^{i\nu\cdot\omega_0\tau_v}\mathcal{B}_{v\nu}, \tag{A.27}$$

with

$$\mathcal{B}_{v\nu} = e^{2m_v\lambda\tau}\left[(-1)^{\delta_v+1}w_{\delta_v}\mathcal{A}_v \prod_{w\,:\,w'=v} w_{r_w}\right]_{\nu_v}, \tag{A.28}$$

where the exponential $e^{2m_v\lambda\tau}$ simply deletes the corresponding $e^{-2m_v\lambda\tau}$ arising from $\mathcal{A}_v$ (see (A.19)).

Then $\nu_v = (\nu_{v1}, \nu_{v2}) \in \mathrm{Z}^2$ is called the *mode label* associated to the node v and represents the Fourier label of the function in (A.22).

For the root we set

$$\mathcal{B}_{r\nu_r} = \begin{cases} w_{1\nu_r} & \text{if } \delta_{v_0} = 2\ , \\ w_{2\nu_r} & \text{if } \delta_{v_0} = 1\ , \end{cases} \tag{A.29}$$

and call $\nu_r \in \mathrm{Z}^2$ the *mode label of the root*.

Define the *momentum* flowing through a line ℓ_v and the *decay label*, respectively, as

$$\nu_{\ell_v} = \sum_{w\preceq v} \nu_v, \qquad k_{\ell_v} = \sum_{w\preceq v} 2m_v. \tag{A.30}$$

In this way we have that the operator $\mathcal{I}$ corresponding to a node v acts as $\mathcal{I}$ applied to the exponential $\exp[i\omega_0\cdot\nu_{\ell_v}\tau_v - k_{\ell_v}\lambda\tau_v]$, i.e. as in (A.10), with $\nu \equiv \nu_{\ell_v}$ and $k = k_{\ell_v}$. Therefore we can represent the value of the tree not by associating to the nodes the $\mathcal{I}$ operators, but using the Fourier expansion (A.27) for the node functions and associating to the any line ℓ exiting from a free node a *propagator*

$$g_\ell \equiv \frac{1}{(i\omega_0\cdot\nu_\ell - k_\ell\lambda)}, \tag{A.31}$$

while we simply set $g_\ell = 1$ if ℓ exits from a leaf.

Finally we shall define the *node factor* and the *root factor*, respectively, as

$$\begin{cases} F_v = \mathcal{B}_{v\nu_v}, & \text{if } v \text{ is a free node}\ , \\ F_v = 1, & \text{if } v \text{ is a leaf}\ , \end{cases} \qquad F_r = \mathcal{B}_{r\nu_r}. \tag{A.32}$$

By writing $y^{(n)}(\tau)$ as in (6.18), then we can write, by also redefining the value of the tree with respect to the previous definition,

$$y^{(n)}_{\nu,k} = \sum_{\theta\in\mathcal{T}^n_{\nu,k}} \mathrm{Val}(\theta), \qquad \mathrm{Val}(\theta) = F_r\left[\prod_{v\in V(\theta)} F_v\right]\left[\prod_{\ell\in\Lambda(\theta)} g_\ell\right], \tag{A.33}$$

if $\mathcal{T}^n_{\nu,k}$ is the set of all trees of order n such that

$$\nu_r + \nu_{\ell_{v_0}} = \nu, \qquad k_{\ell_{v_0}} = k, \tag{A.34}$$

if $\nu_{\ell_{v_0}}$ is the momentum flowing through the root line, ν_r is the mode label of the root and $k_{\ell_{v_0}}$ is the decay label associated to the root line. Note that $k = n_0 \le n$.

Now it is easy to show that for all trees $\theta \in \mathcal{T}^n_{\nu,k}$, one has

$$\sum_{\{\nu_v\}_{v\in\theta}} \left| F_r \prod_{v\in V(\theta)} F_v \right| \le B_1 C_1^n e^{-k'|\nu|}, \tag{A.35}$$

for some constants $k' \in (0,\kappa)$ and B_1, C_1 positive, while the number of trees in $\mathcal{T}^n_{\nu,k}$ with fixed mode labels is bounded by C_2^k for some constant C_2; the summability on $\{\nu_v\}$ in (A.35) can be performed

(neglecting the constraint that a momentum $\nu - \nu_r$ has to flow through the root line) by using the property (6.10), in a standard way; see for instance [15].

Moreover one has

$$|g_\ell| \leq \frac{1}{\lambda}, \tag{A.36}$$

as $k_\ell \geq 2$ (see (A.30)): in particular no condition has to be imposed on the rotation vector ω_0. In terms of the parameters ω, b, we require only that they lay inside the lowest stability region.

By collecting together all the bounds found above, we have that

$$\left| y^{(n)} \right| \leq B_0 C_1^n C_2^n \lambda^{-n}, \tag{A.37}$$

for some constant B_0 so that the series (A.1) defining $y(\tau;\varepsilon)$ converges for $|\varepsilon| < \varepsilon_0 = O(\lambda)$.

The discussion in this section leads to the following result stating the asymptotic stability of the position $(y, \dot{y}) = (0, 0)$. Given the equation (6.5), assume that the parameters ω and b are such that (6.19) is satisfied; then there exists $\varepsilon_0 > 0$ such that the equilibrium position $(y, \dot{y}) = (0, 0)$ is the ω-limit set of any initial datum $(y(0), \dot{y}(0))$ satisfying $y^2(0) + \dot{y}^2(0) < \varepsilon_0^2$. In particular the ball of center $(0, 0)$ and radius ε_0 is contained inside the basin of attraction of $(0, 0)$. One has $\varepsilon_0 = O(\lambda)$. By the discussion in Sect. 6 this implies the Theorem (recall also that $\delta = \sqrt{\varepsilon}$, for $\varepsilon \in \mathrm{R}^+$).

Acknowledgements

We thank Peter Ashwin and John R Terry for use of their numerical program for computing the basins of attractions. We also thank Philip J Aston, Philip Kent, Sebastian Reich and John R Terry for their help with the numerics and for useful discussions.

References

[1] D. J. Acheson, *A pendulum theorem*, Proc. R. Soc. Lond. A **443** (1993), 239–245.

[2] D. J. Acheson, *Multiple-nodding oscillations of a driven inverted pendulum*, Proc. R. Soc. Lond. A **448** (1995), 89–95.

[3] D. Acheson, *From calculus to chaos*, Oxford University Press, Oxford, 1997.

[4] D. J. Acheson & T. Mullin, *Upside-down pendulums*, Nature **366** (1993), 215–216.

[5] F. M. Arscott, *Periodic differential equations*, Pergamon Press, Oxford, 1964.

[6] B. L. Baker & J. P. Gollub, *Chaotic dynamics. An introduction*, Cambridge University Press, Cambridge, 1996.

[7] M. V. Bartuccelli, G. Gentile & K. V. Georgiou, *KAM theorem and stability of the upside-down pendulum*, Preprint (2000).

[8] J. A. Blackburn, H. J. T. Smith & N. Grønbech-Jensen, *Stability and Hopf bifurcations in an inverted pendulum*, Amer. J. Phys. **60** (1992), 903–908.

[9] J. A. Blackburn, H. J. T. Smith & D. E. Edmundson, *Transient chaos in a parametrically damped pendulum*, Phys. Rev. A **45** (1992), 593–599.

[10] G. Blanch, *Mathieu functions*, in M. Abromowitz & I. A. Stegun, *Handbook of mathematical functions*, Dover, New York, 1965.

[11] D. Capecchi & S. R. Bishop, *Periodic oscillations and attracting basins for a parametrically excited pendulum*, Dynam. Stability of Systems **9** (1994), 123–143.

[12] R. Doerner, B. Hübinger, H. Heng & W. Martienssen, *Approaching nonlinear dynamics by studying the motion of a pendulum. II. Analyzing chaotic motion*, Internat. J. Bifur. Chaos Appl. Sci. Engrg. **4** (1994), 761–771.

[13] J.-P. Eckmann & D. Ruelle, *Ergodic theory of chaos and strange attractors*, Rev. Mod. Phys. **57** (1985), 617–656.

[14] G. Gentile, *Whiskered tori with prefixed frequencies and Lyapunov spectrum*, Dynam. Stability of Systems **10** (1995), 269–308.

[15] G. Gentile & V. Mastropietro, *Methods for the analysis of the Lindstedt series for KAM tori and renormalizability in classical mechanics. A review with some applications*, Rev. Math. Phys. **8** (1996), 393–444.

[16] C. Grebogi, E. Ott, J. A. Yorke, *Critical exponent of chaotic transients in nonlinear dynamical systems*, Phys. Rev. Lett. **57** (1986), 1284–1287.

[17] E. Gröller, *Application of Visualization tehniques to complex and chaotic dynamical systems*, Preprint (1994).

[18] M. Guzzo, F. Fassò & G. Benettin, *On the stability of elliptic equilibria*, Math. Phys. Electron. J. **4** (1998), Paper 1, 1–16.

[19] F. Harary & E. Palmer, *Graphical enumerations*, Academic Press, New York, 1973.

[20] K. M. Heal, M. L. Hansen & K. M. Rickard, *Maple V learning guide*, Springer, 1996.

[21] H. Heng, R. Doerner, B. Hübinger & W. Martienssen, *Approaching nonlinear dynamics by studying the motion of a pendulum. I. Observing trajectories in state space*, Internat. J. Bifur. Chaos Appl. Sci. Engrg. **4** (1994), 751–760.

[22] M. Henon, *On the numerical computation of Poincaré Maps*, Phys. D **5** (1982), 412–414.

[23] C. W. Hilborn, *Chaos and nonlinear dynamics*, Oxford University Press, Oxford, 1994.

[24] D. W. Jordan & P. Smith *Nonlinear ordinary differential equations*, Clarendon Press, Oxford, 1977.

[25] H. P. Kalmus, *The inverted pendulum*, Amer. J. Phys. **38** (1970), 874–878.

[26] P. L. Kapitsa, *Dynamic stability of a pendulum with a vibrating point of suspension*, Zh. Ehksp. Teor. Fiz. **21** (1951), 588–598 (Russian), translated version in *Collected papers by P. L. Kapitsa*, edited by D. ter Haar, Pergamon, Vol. 2, 714–726, London, 1965.

[27] B. P. Koch, R. W. Leven, B. Pompe & C. Wilke, *Experimental evidence for chaotic behaviour of a parametrically forced pendulum*, Phys. Lett. A **96** (1983), 219–224.

[28] B. P. Koch & R. W. Leven, *Subharmonic and Homoclinic bifurcations in a parametrically forced pendulum*, Phys. D **16** (1985) 1–13.

[29] L. D. Landau, E. M. Lifshitz, *Mechanics*, 3rd Edn, Pergamon Press, Oxford, 1976.

[30] T. Leiber & H. Risken, *Stability of parametrically exited dissipative systems*, Phys. Lett. A **129** (1988), 214–218.

[31] R. W. Leven & B. P. Koch, *Chaotic behaviour of a parametrically excited damped pendulum*, Phys. Lett. A **86** (1981), 71–74.

[32] R. W. Leven, B. Pompe, C. Wilke & B. P. Koch, *Experiments on periodic and chaotic motions of a parametrically forced pendulum*, Phys. D **16** (1985), 371–384.

[33] M. M. Michaelis, *Stroboscopic study of the inverted pendulum*, Am. J. Phys **53** (1985), 1079–1083.

[34] M. B. Monagan, K. O. Geddes, G. Labahn & S. Vorkoetter, *Maple V programming guide*, Springer, 1996.

[35] D. J. Ness, *Small oscillations of a stabilized, inverted pendulum*, Amer. J. Phys. **35** (1967), 964–967.

[36] I. Percival & D. Richards, *Introduction to dynamics*, Cambridge University Press, Cambridge, 1982.

[37] A. B. Pippard, *The inverted pendulum*, European J. Phys. **8** (1987), 203–206.

[38] H. Poincaré, *Les Méthodes Nouvelles de la Méchanigue Céleste*, Vol. III, Gauthiers-Villars, Paris, 1899.

[39] H. J. T. Smith & J. A. Blackburn, *Chaos in a parametrically damped pendulum*, Phys. Rev. A **40** (1989), 4708–4715.

[40] H. J. T. Smith & J. A. Blackburn, *Experimental study of an inverted pendulum*, Amer. J. Phys. **60** (1992), 909–911.

[41] A. Stephenson, *On a new type of dynamical stability*, Mem. Proc. Manch. Lit. Phil. Soc. **52** (1908), 1–10.